NRC Research Press

ARTICLE

Theoretical calculations of rate of NDMA formation from gramine

F. Shojaie and M. Dehestani

Abstract: The first *ab initio* theoretical study is performed on the ion–molecule reaction of gramine ($C_{11}H_{14}N_2$) with NO^+ for the formation of *N*-nitrosodimethylamine (NDMA). The reaction mechanism is investigated using the B3LYP density functional theory level. The stationary points along the reaction energy profile have been calculated at the B3LYP/6-311+G(d,p) level of the theory in the gas phase and solution phase. In this work, an attempt is made to elucidate the mechanism and so is proposed the efficient reactive pathway for the reaction of gramine with NO^+ step by step. A complete reaction mechanism has been established, and the temperature dependence of all rate constants between 23 and 65 °C are reported and analyzed in terms of transition state theory. The percentages of NDMA formation in the 23–65 °C temperature range have been calculated in aqueous solution by transition state theory. The results are in good agreement with experimental results.

Key words: gramine, *N*-nitrosodimethylamine, rate constant, variational transition state.

Résumé : On a effectué la première étude théorie *ab initio* de la réaction ion–molécule de la gramine ($C_{11}H_{14}N_2$) avec le cation NO^+ qui conduit à la formation de *N*-nitrosodiméthylamine (NDMA). On a étudié le mécanisme réaction au niveau B3LYP de la théorie de la fonctionnelle de la densité. Les points stationnaires le long du profil de l'énergie potentielle ont été calculés au niveau B3LYP/6-311+G(d,p) de la théorie, tant en phase gazeuse qu'en solution. Dans ce travail, on a essayé d'élucider le mécanisme et, à cette fin, on suggère étape par étape quelle est la voie réactive efficace pour la réaction de la gramine avec NO^+. Un mécanisme réactionnel complet a été établi; on a déterminé la relation entre la température et toutes les constantes de vitesse entre 23 et 65 °C et elle a été analysée en fonction de la théorie de l'état de transition. Faisant appel à la théorie de l'état de transition, on a calculé les pourcentages de formation de NDMA, en solution aqueuse, à des températures allant de 23 à 65 °C. Les résultats des calculs sont en bon accord avec les données expérimentales. [Traduit par la Rédaction]

Mots-clés : gramine, *N*-nitrosodiméthylamine, constante de vitesse, état de transition variationnel.

Introduction

In 1956, Magee and Barnes[1] reported that *N*-nitrosodimethylamine (NDMA) could induce liver cancer when it was fed to rats. Afterwards, there was a great deal of experimental studies on the chemical properties, metabolism, and carcinogenicity of nitrosamines.[2–5] NDMA can be formed during food processing, preservation, and preparation from precursor compounds already present in, or added to, the specific food items and it has been detected in cured meats, fired bacon, seafood, dried milk products, and beer.[6,7] It is well recognized that beer may contain trace amounts of NDMA, a highly active carcinogen. Most malt beverages, including beer and most brands of whiskey, regardless of origin, contain NDMA. The presence of NDMA in beer was first reported in 1979.[8] Examination of beer from different sources revealed that malt was the main source of NDMA contamination in beer.[9] Reaction of oxides of nitrogen with certain alkaloids during the direct-fire drying step of the malting process has been established as the major pathway for the formation of *N*-nitrosamines in beer.[10] Previous investigations have reported NDMA levels in beer derived from the barley malt. Alkaloids (hordenine, gramine ($C_{11}H_{14}N_2$)) formed in malt roots during germination may act as amine precursors in nitrosation. The experimental results have demonstrated that the rate of gramine nitrosation to NDMA is faster than the rate of hordenine nitrosation to NDMA under various conditions of pH and temperature.[11] The comparison of these rates at 23, 37, and 65 °C has shown that gramine is much more highly susceptible to nitrosation to produce NDMA. Gramine has been formed biosynthetically from tryptophan and found in malt acrospires (shoots) after germination.[12] The rate of gramine nitrosation and the nature of the nitrosation products indicate that gramine does not undergo nitrosation by the expected mechanism of nitrosative dealkylation.[13] The reaction sequence for NDMA formation is shown in Fig. 1.[14]

In this work, we use high-level *ab initio* calculations to investigate reaction mechanisms for formation of NDMA from gramine. Until now, to the best of our knowledge, no previous theoretical work has been devoted to the study of the mechanism of the reaction of gramine with NO^+. In this paper, an attempt is made to elucidate the mechanism and to propose the efficient reactive pathway for the reaction of gramine with NO^+ step by step. This pathway scheme can be clarified as follows:

$$[1] \quad C_{11}H_{14}N_2 + NO^+ \rightarrow IM1 \rightarrow TS1 \rightarrow IM2 \rightarrow TS2 \rightarrow IM3 \rightarrow [C_9H_8N]^+ + NDMA$$

Calculations have been performed for this reaction in the gas phase and in the solution phase. We should mention that no experimental results have been reported to date in the gas phase, so comparison with the experimental results cannot be made at the present time. However, results are in good agreement with the experimental results in the solution phase.

Computational methods

For the $C_{11}H_{14}N_2 + NO^+$ reaction, the geometries of the reactants, the products, the intermediates, and the transition states are fully

Received 12 June 2012. Accepted 13 August 2012.

F. Shojaie. Department of Photonics, Graduate University of Advanced Technology, Kerman, Iran.
M. Dehestani. Department of Chemistry, Shahid Bahonar University of Kerman, Kerman, Iran.
Corresponding author: F. Shojaie (e-mail: fahimeh_shojaie@yahoo.com).

Fig. 1. NDMA formation in beer from gramine.[14]

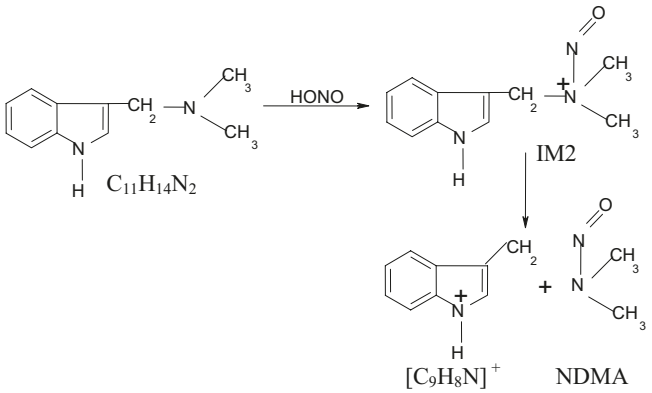

optimized at the B3LYP/6-311+G(d,p) level.[15] The harmonic vibrational frequency calculations are performed at the same level. Each transition state is verified to connect the designated reactants with products by performing an intrinsic reaction coordinate analysis.[16–18] The minimum energy paths are obtained by intrinsic reaction coordinate calculations. Solvation model including polarizable continuum model (PCM) and atomic radii including Bondi are used at the B3LYP/6-311+G(d,p) level. All calculations are performed using the GAUSSIAN 03 software package.[19] Finally, the theoretical rate constants in the temperature range from 290 to 360 K are calculated using the transition state theory[20,21] in the gas phase and in the solution phase.

Results and discussion

Calculations in the gas phase

For the $C_{11}H_{14}N_2$ + NO^+ reaction, optimized structures for the stationary points along the reaction coordinate (reactants, transition states, intermediates, and products) are collected in Fig. 2 and the corresponding potential energy surface is shown in Fig. 3. As shown in Fig. 3, the intermediate from reactant occurs without an exit barrier. The formation of the addition complex IM1 is due to the electrostatic effect of the $C_{11}H_{14}N_2$ close up to the NO^+. When compared with the structures of the isolated reactants, as shown in Fig. 2, both gramine and NO^+ in the precursor complexes are in the same plane with each other and the geometries are nearly unchanged and take on a more reactant-like character. The pathway for the reaction of $C_{11}H_{14}N_2$ with NO^+ consists of two reaction steps. The first step is an NO^+ addition to gramine (IM1) and formation of IM2 (IM1 → IM2) and the second step is the production of NDMA (IM2 → IM3). In the second step (IM2 → IM3), the C16–N27 bond breaking yields IM3 via transition state TS2.

The Gibbs free energies, reaction enthalpies, and imaginary vibrational frequencies calculated at the B3LYP/6-311+G(d,p) theory level in the gas phase are given in Table 1.

The changing of some calculated key bond lengths along the reaction coordinate for the first step and for the second step is shown in Fig. 4.

We explain in detail this changing for the first and second steps. It appears that N27–N29 and C16–N27 bonds change strongly during the course of the reaction and the other bond lengths are almost invariant during the reaction coordinate. In the first step (IM1 → IM2), the bond length N27–N29 is almost unchanged from $s = -\infty$ $(amu)^{1/2}$ bohr to $s = -0.4$ $(amu)^{1/2}$ bohr and equals the value of this bond in IM1 and then shortens after about $s = -0.4$ $(amu)^{1/2}$ bohr and arrives at the bond length of N27–N29 in IM2, and then this bond becomes constant in the second step (IM2 → IM3). The C16–N27 bond is constant in the first step but in the second step, the bond length is almost unchanged from $s = -\infty$ $(amu)^{1/2}$ bohr to $s = -1$ $(amu)^{1/2}$ bohr and equals the value of this bond in IM2 and then elongates after about $s = -1$ $(amu)^{1/2}$ bohr and arrives at the bond length of C16–N27 in IM3.

The classical potential energy (V_{MEP}), the ground-state vibrational adiabatic potential energy (V_a^G), and the zero-point energy (ZPE) for the reaction IM2 → IM3 as functions of the intrinsic reaction coordinates are calculated (where $V_a^G(s) = V_{MEP}(s) +$ ZPE(s)). Figure 5 shows the plots of V_{MEP}, V_a^G, and ZPE versus reaction coordinate.

The position of the maximum of $V_{MEP}(s)$ is almost the same as that of $V_a^G(s)$, and thus, the ZPE curve is constant in the vicinity of the saddle point as shown in Fig. 5. To analyze this behavior in more detail, we present the variations of generalized normal mode vibrational frequencies along the minimum energy path (MEP) for reaction IM2 → IM3 in Fig. 6. Since there are 81 vibrational frequencies of the optimized stationary points for this reaction, for simplicity, only some of them have been shown in Fig. 6. In the negative limit of s ($s = -\infty$), the frequencies correspond to the reactants, while in the positive limit of s ($s = +\infty$), the frequencies are associated with the products. For clarity, the vibrational frequencies can be divided into three types: spectator modes, transition modes, and reactive modes.

The spectator modes are those in which their frequency undergoes little change from reactants to the transition state. The lowest vibrational frequencies are related to transition modes. These frequencies tend to be zero at the reactant and product limit and reach their maximum value in the saddle point zone. The reactive modes are those that undergo the largest change in the saddle point zone, and therefore, they must be related to the breaking or forming of bonds. In Fig. 6, the solid line 2 represents symmetric bending frequency of C15–C16–N27; it drops linearly after the saddle point($s = 0$) and goes to zero for product. The mode shown by the solid line 1, which relates to the breaking of the C16–N27 bond in the reactant region and the forming of the N27–N29 bond in the product region, changes sharply in the region from $s = -1.0$ to 1.0 $(amu)^{1/2}$ bohr and is reactive mode. These changes should cause decreases in the ZPE. The solid line 3, which corresponds to free translations of the reactant, represents the lowest frequency (transition mode). As a result, ZPE has little change with s. Therefore, the classical potential energy (V_{MEP}) and the ground-state vibrational adiabatic potential energy (V_a^G) have similar shapes.

In addition, Fig. 3 demonstrates the schematic the Gibbs free energy profiles. As shown in Fig. 3, since Gibbs free energies of all stationary points lie below that of the reactants $C_{11}H_{14}N_2$ and NO^+, this pathway should occur easily even at low-temperature conditions in the gas phase. It is in good agreement with the experimental results.[11] Figure 3 shows both IM1 and IM2 complexes and transition states are located below the reactants energy level and TS2 is more unstable than IM1. The rate constants are calculated for each step, IM1 → IM2 ($k_{1\to2}$) and IM2 → IM3 ($k_{2\to3}$), by transition state theory as follows:[21]

$$[2] \qquad k_g = \frac{k_B T}{h} \exp\left(-\frac{\Delta G_g^{\neq}}{RT}\right)$$

in which $\Delta G_g^{\neq}$ denotes the difference between Gibbs free energies of reactants and transition state (including zero point energy) in the gas phase, R is the universal gas constant, and T is the temperature. The calculated rate constants for each step in the temperature range of 290–360 K at the B3LYP/6-311+G(d,p) level are given in Table 2 and Fig. 7.

To obtain the overall rate constant in the gas phase, we supposed that the reaction occurs in only one step, IM1 → IM3 via TS2. Thus, pathway scheme (eq. 1) can be clarified as follows:

$$[3] \qquad C_{11}H_{14}N_2 + NO^+ \rightarrow IM1 \rightarrow TS2 \rightarrow IM3 \rightarrow [C_9H_8N]^+ + NDMA$$

Fig. 2. Optimized geometries of all of the reactants, intermediates, transition states, and products for the $C_{11}H_{14}N_2$ + NO^+ reaction at the B3LYP/6-311+G(d,p) level. Bond lengths are in angströms and angles are in degrees.

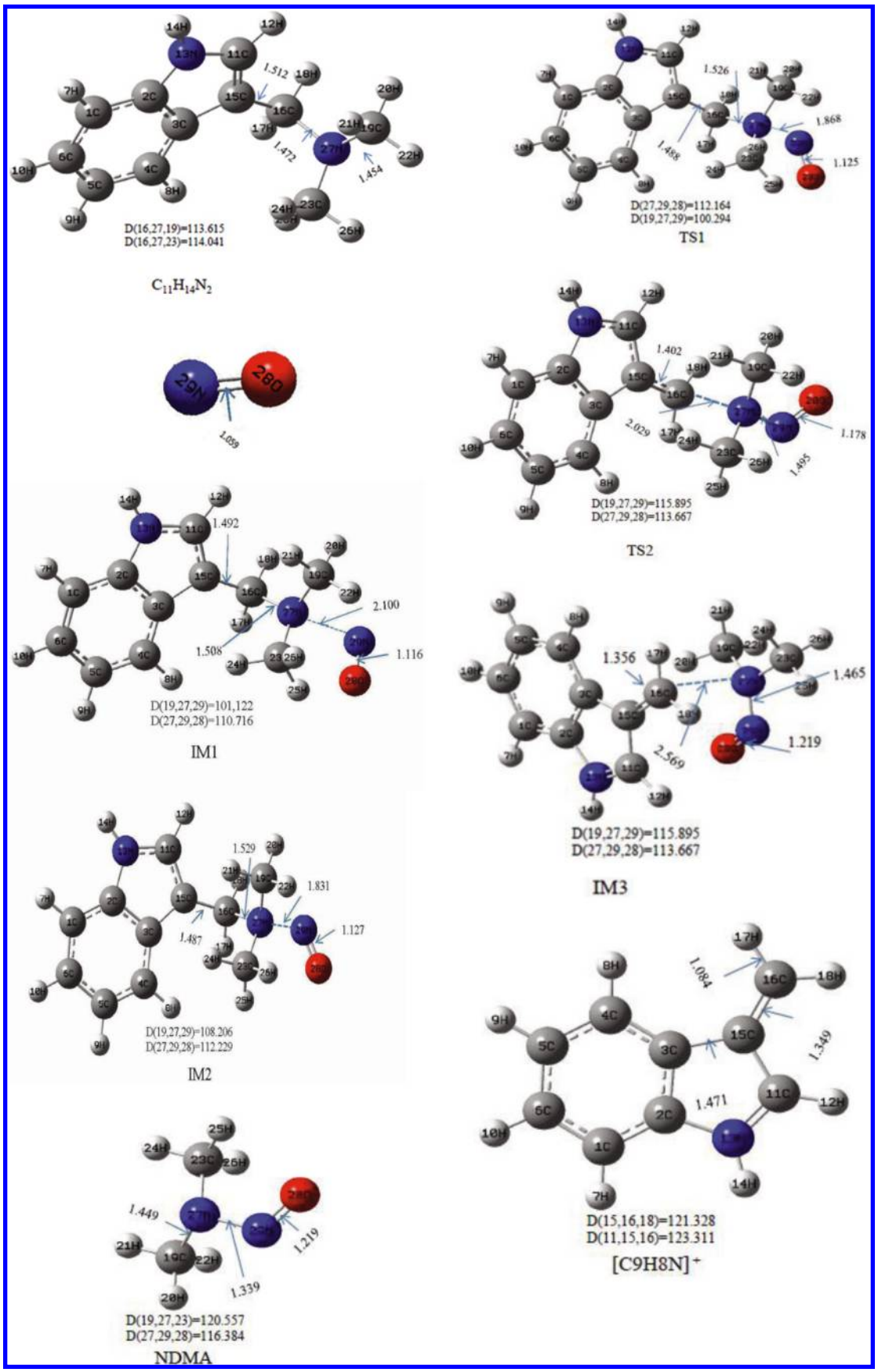

Fig. 3. Gibbs free energy changes along the reaction pathway at the B3LYP/6-311+G(d,p) level of theory in the gas phase. Energies are in kcal mol^{-1}.

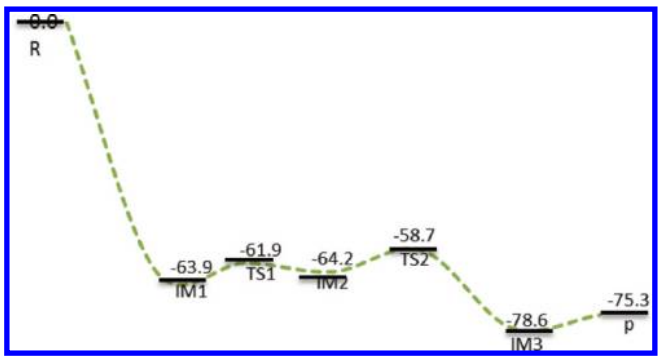

Table 3 presents the Gibbs free energies and enthalpy and Table 4 shows total rate constant ($k_{t(g)}$) for IM1 → IM3 in the gas phase at the B3LYP/6-311+G(d,p) level. Figure 8 shows that the branching fractions $k_{1\rightarrow2}/k_{t(g)}$ and $k_{2\rightarrow3}/k_{t(g)}$ are dependent on temperature. The total rate constant $k_{t(g)}$ is nearly equal to the rate constant $k_{2\rightarrow3}$, as shown in Fig. 8. Therefore, the rate-determining step of NDMA formation is IM2 → IM3. There are no experimental values for comparison with our theoretical results.

Calculations in the solution phase

The equations for the formation of the nitrosonium ion (NO^{+}) in solutions of nitrous acid areas follows:

$$[4] \qquad H^+ + HNO_2 \rightleftharpoons H_2NO_2^+ \quad K_1 = \frac{[H_2NO_2^+]}{[H^+][HNO_2]}$$

$$[5] \qquad H_2NO_2^+ \rightleftharpoons NO^+ + H_2O \quad K_2 = \frac{[NO^+]}{[H_2NO_2^+]}$$

Kinetic evidence[22] shows that $H_2NO_2^+$ may be an important nitrosating species in aqueous diazotization. It seems reasonable to suppose that $H_2NO_2^+$ is formed rapidly from molecular nitrous acid by a proton transfer, but its equilibrium concentration may be small. Thus, NO^+ is produced according to the following reaction:

$$[6] \qquad H^+ + HNO_2 \rightleftharpoons NO^+ + H_2O \quad K_3 = \frac{[NO^+]}{[H^+][HNO_2]}$$

where K_1, K_2, and K_3 are equilibrium constants of reactions 4, 5, and 6, respectively. In these equations, the concentration of H_2O is constant. Since reaction 6 is the sum of reactions 4 and 5, we can thus write $K_3 = K_1K_2$.

We now turn to the NDMA formed in the reaction of $C_{11}H_{14}N_2$ with NO^+ (eq. 3); the rate of reaction is given by

$$[7] \qquad \text{Rate} = k_{t(s)}[NO^+][C_{11}H_{14}N_2]$$

where $k_{t(s)}$ is the rate constant of the reaction in the solution phase.

Substituting of concentration NO^+ from eq. 6 into eq. 7, we obtain eq. 8:

$$[8] \qquad \text{Rate} = k_{t(s)}K_3[C_{11}H_{14}N_2][H^+][HNO_2]$$

The experimental evidence of Mangino et al.[11] showed that the formation of NDMA from gramine is pseudo-first-order. For a pH and constant concentration of nitrous acid, we can write the overall rate of NDMA formation as follows:

$$[9] \qquad \text{Rate} = k[C_{11}H_{14}N_2]$$

where k is the pseudo-first-order rate constant for the NDMA formation reaction in the solution phase (in the presence of water) and depends on the concentration of nitrous acid and pH.

By comparing eqs. 8 and 9, we can then write

$$[10] \qquad k = k_{t(s)}K_3[H^+][HNO_2]$$

As can be seen from eq. 10, to calculate k, nitrous acid concentration, pH, K_3, and $k_{t(s)}$ are required. We used equilibrium constant K_{HNO_2} to calculate the nitrous acid concentration according to the following well-known reaction:

$$[11] \qquad HNO_2 \rightleftharpoons NO_2 + H^+ \quad K_{HNO_2} = \frac{[NO_2^+][H^+]}{[HNO_2]} = 6.3 \times 10^{-4} \text{ mol L}^{-1}$$

In this work, the concentration of HNO_2 is calculated at pH = 3.4 and NO_2^- = 1.0 mol L^{-1}.[11]

Theoretical calculation of $k_{t(s)}$

The rate constant of reaction in the solution phase ($k_{t(s)}$) is calculated based on transition state theory using the well-known formula

$$[12] \qquad (k_{t(s)}) = \frac{k_BT}{h}\exp\left(\frac{-\Delta G_s^{\neq}}{RT}\right)$$

The free energy change in solution ($\Delta G_s^{\neq}$) is obtained according to the following equation:

$$[13] \qquad \Delta G_s^{\neq} = \Delta G_g^{\neq} + \Delta G_{sol}^{\neq}$$

where $\Delta G_{sol}^{\neq}$ and $\Delta G_g^{\neq}$ are solvation and the gas-phase free energy changes, respectively.

Substituting eq. 13 into eq. 12 and combining the results into eq. 2, we obtain

$$[14] \qquad (k_{t(s)}) = k_{t(g)}\exp\left(\frac{-\Delta G_{sol}^{\neq}}{RT}\right)$$

The free energy changes and the rate constant in the solution phase are calculated at the highest level of theory (B3LYP/6-311+G(d,p)) with the PCM method and are collected in Table 5.

Theoretical calculation of K_3

The standard-state free energy change associated with the reaction in solution represented in eq. 6 (ΔG_s^0) is related to the equilibrium constant K_3 according to the following equation:

$$[15] \qquad pK_3 = \frac{\Delta G_s^0}{RT \ln 10}$$

Using the thermodynamic cycle shown in Fig. 9 and theoretical techniques, the free energy change of this reaction can be written as

$$[16] \qquad \Delta G_s^0 = \Delta G_g^0 + \Delta G_{sol}^0(NO^+) + \Delta G_{sol}^0(H_2O) - \Delta G_{sol}^0(HNO_2) - \Delta G_{sol}^0(H^+)$$

Table 1. Gibbs free energies, reaction enthalpies, and imaginary vibrational frequencies (cm^{-1}) for the first step and for the second step.

	Gas phase							
	IM1 → IM2				IM2 → IM3			
Level	ΔG^0_{298}	ΔH^0_{298}	$\Delta G^{\neq}$	ω	ΔG^0_{298}	ΔH^0_{298}	$\Delta G^{\neq}$	ω
B3LYP/6-311+G(d,p)	−0.3	−0.5	2.0	157.0*i*	−14.4	−12.7	5.5	286.9*i*

Note: Energies are in kcal mol^{-1}.

Fig. 4. The changing of some key bond distances along the reaction coordinate for the first step of the reaction.

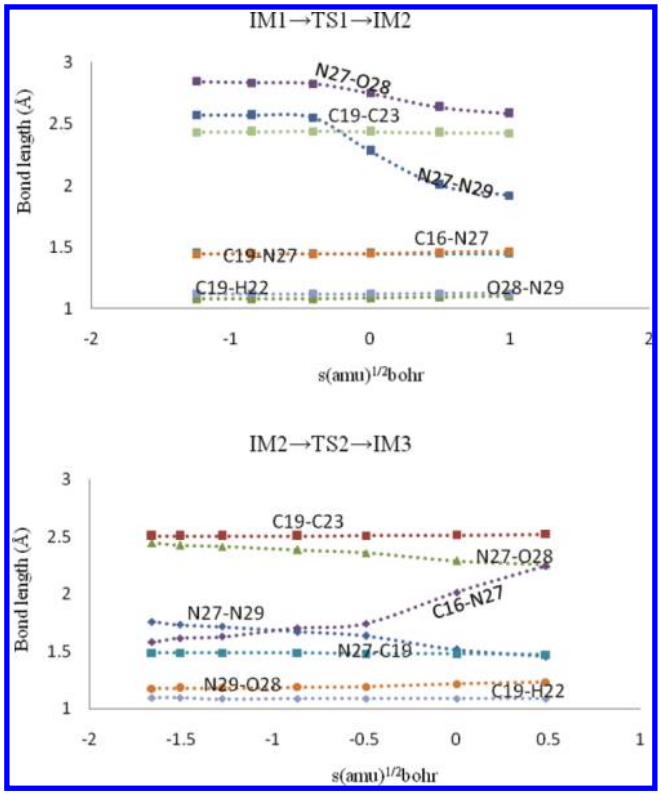

Fig. 5. Classical potential energy (V_{MEP}), vibrational adiabatic potential energy (V_a^G), and ZPE as functions of the intrinsic reaction coordinate, *s*, at the B3LYP/6-311+G(d,p) level of theory for the reaction IM2 → IM3.

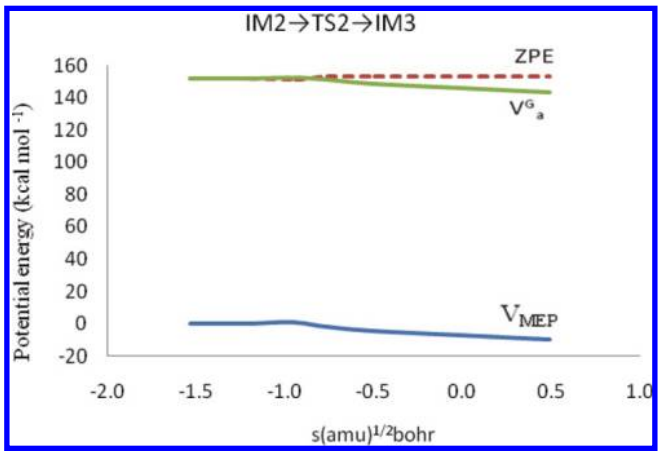

Fig. 6. Change of the generalized normal-mode vibrational frequencies for the IM2 → IM3 reaction as functions of the reaction coordinate, *s*, at the B3LYP/6-311+G(d,p) level.

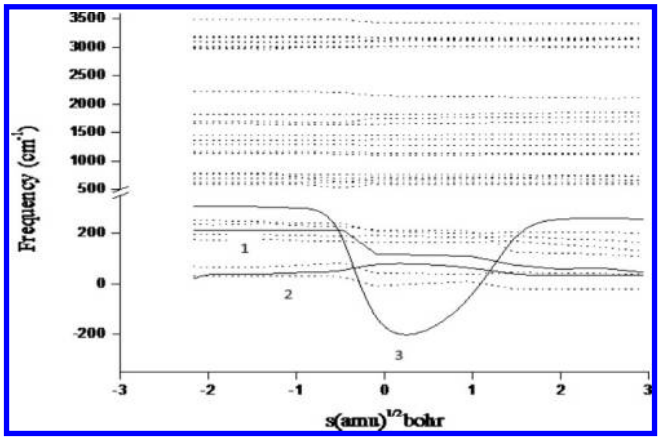

Table 2. Calculated rate constants for the first step and for the second step.

	Gas phase	
T (K)	B3LYP/6-311+G(d,p) $k_{1\to2}$ (s^{-1})	B3LYP/6-311+G(d,p) $k_{2\to3}$ (s^{-1})
290	2.18 (11)	4.95 (8)
296	2.20 (11)	5.70 (8)
297	2.23 (11)	5.73 (8)
310	2.36 (11)	9.21 (8)
338	2.85 (11)	2.84 (9)
360	3.16 (11)	5.42 (9)

Note: Values in parentheses denote power of 10.

Fig. 7. Calculated transition state theory rate constants as a function of $10^3/T$ for reactions M1 → IM2 (k_1) and IM2 → IM3 (k_2) at the B3LYP/6-311+G(d,p) level in the gas phase.

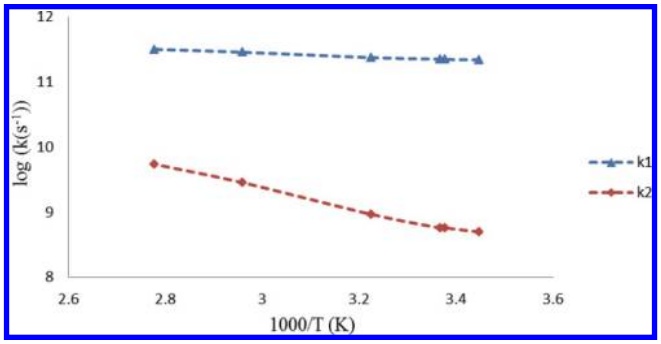

Table 3. Gibbs free energies and reaction enthalpies for IM1 → IM3.

	Gas phase IM1 → IM3		
Level	ΔG^0_{298}	ΔH^0_{298}	$\Delta G^{\neq}$
B3LYP/6-311+G(d,p)	–14.7	–13.2	5.2

Note: Energies are in kcal mol^{-1}.

Table 4. Calculated rate constants for IM1 → IM3 in the gas phase.

	Gas phase B3LYP/6-311+G(d,p)
T (K)	$k_{1\rightarrow3} = k_{t(g)}$ (s^{-1})
290	5.79 (8)
296	8.53 (8)
297	8.99 (8)
310	1.03 (9)
338	2.10 (9)
360	3.34 (9)

Note: Values in parenthesis denote power of 10.

Fig. 8. The logarithm of calculated branching ratio for the reaction $C_{11}H_{14}N_2$ + NO$^+$ as a function of $10^3/T$ at the B3LYP/6-311+G(d,p) level in the gas phase.

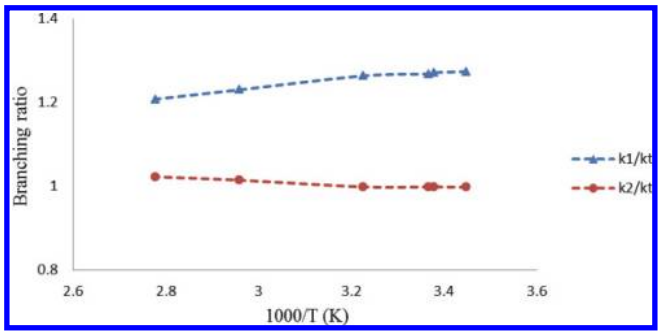

where ΔG^0_g is the standard-state gas-phase free energy change and ΔG^0_{sol} is the standard-state solvation free energy. ΔG^0_g is defined by

$$[17] \qquad \Delta G^0_g = G^0_g(NO^+) + G^0_g(H_2O) - G^0_g(HNO_2) - G^0_g(H^+)$$

To obtain the standard-state gas-phase free energies of all species involved in this reaction, we performed geometry optimization of these species using the HF/6311++G(3df,3pd) theory level. The Gaussian 03 program was employed for the *ab initio* calculations. Free energies of solvation were calculated using the solvent model including the dielectric polarizable continuum (DPCM).[23–25] To emulate these calculations in Gaussian 03, which has a dramatically different default PCM implementation, the solvent keyword DPCM was used with the setting ICOMP = 4.[26] The optimized atomic radii were invoked via the solvent keyword RADII = UAHF. Solvation free energies were then obtained using the SCFVAC keyword at the HF/6-311++G(3df,3pd) theory level. The free energy of solvation of H$^+$ (ΔG^0_{sol}) has been considered as –1104.5 kJ mol^{-1}.[27] The equilibrium constants K_3 and ΔG^0_s in a temperature range of 290–360 K for this reaction are collected in Table 6.

The rate constants of NDMA formation from gramine (k) have been calculated from eq. 10 at 23, 24, 37, and 65 °C with 1.0 mol L^{-1} nitrite at pH 3.4. Since the reaction is first order, changes of concentration of gramine with time (t) can be expressed as

$$[18] \qquad [C_{11}H_{14}N_2]_t = [C_{11}H_{14}N_2]_0\, e^{-kt}$$

Table 5. Calculated rate constants $k_{t(s)}$ (s^{-1} M^{-1}), $\Delta G^{\neq}_s$ (kcal mol^{-1}), and the dielectric constant of water and at the B3LYP/6-311+G(d,p) levels in the temperature range 290–360 K.

T (K)	$k_{t(s)}$	$\Delta G^{\neq}_s$	Dielectric constant
290	4.46 (6)	9.96	81.2
296	4.51 (6)	10.18	78.8
297	4.82 (6)	10.18	78.4
310	8.12 (6)	10.36	73.2
338	3.41 (7)	10.45	62.0
360	3.93 (7)	11.12	53.2

Note: Values in parenthesis denote power of 10.

Fig. 9. Thermodynamic cycle for the determination of the standard-state free energy change of the reaction $H^+ + HNO_2 \rightleftharpoons NO^+ + H_2O$ in the solution.

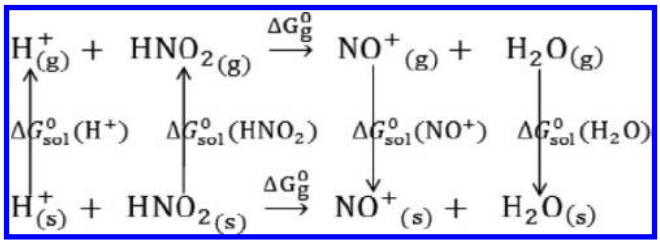

Table 6. Calculated equilibrium constants K_3 (M^{-1}), ΔG^0_s (kcal mol^{-1}), and the dielectric constant of water for the reaction $H^+ + HNO_2 \rightleftharpoons NO^+ + H_2O$ at the HF/6-311++G(3df,3pd) level in the aqueous phase.

T (K)	K_3	ΔG^0_s	Dielectric constant
290	3.42 (–07)	10.42	81.2
296	4.66 (–07)	10.45	78.8
297	4.85 (–07)	10.46	78.4
310	8.99 (–07)	10.54	73.2
338	2.72 (–06)	10.75	62.0
360	5.19 (–06)	10.99	53.2

where $[C_{11}H_{14}N_2]_0$ corresponds to the initial concentration of gramine. The concentration of NDMA generated from the reaction of gramine with NO$^+$ is given by

$$[19] \qquad [NDMA]_t = [C_{11}H_{14}N_2]_0 - [C_{11}H_{14}N_2]_t$$

The percentage of formation of NDMA can be obtained by

$$[20] \qquad \%\ \text{formation of NDMA} = \frac{[NDMA]_t}{[NDMA]_T} \times 100$$

where $[NDMA]_T$ is the total concentration of formed NDMA.

Figure 10 shows the plots of percent formation of NDMA from gramine versus time with 0.1 mol L^{-1} nitrite and pH = 3.4 at 23, 24, 37, and 65 °C and compares with experimental results. The agreement between theoretical and experimental results[11] is satisfactory.

Conclusions

This theoretical work has helped us gain further insight into the gas-phase and solution-phase reaction of NO$^+$ with $C_{11}H_{14}N_2$. In this work, we studied the mechanism for NDMA formation

Fig. 10. Rates of NDMA formation from gramine at 23, 24, 37, and 65 °C with 1.0 mol L^{-1} nitrite at pH 3.4 in the solution phase. Curve *a*, this work; curve *b*, rMangino and Scanlan.[11]

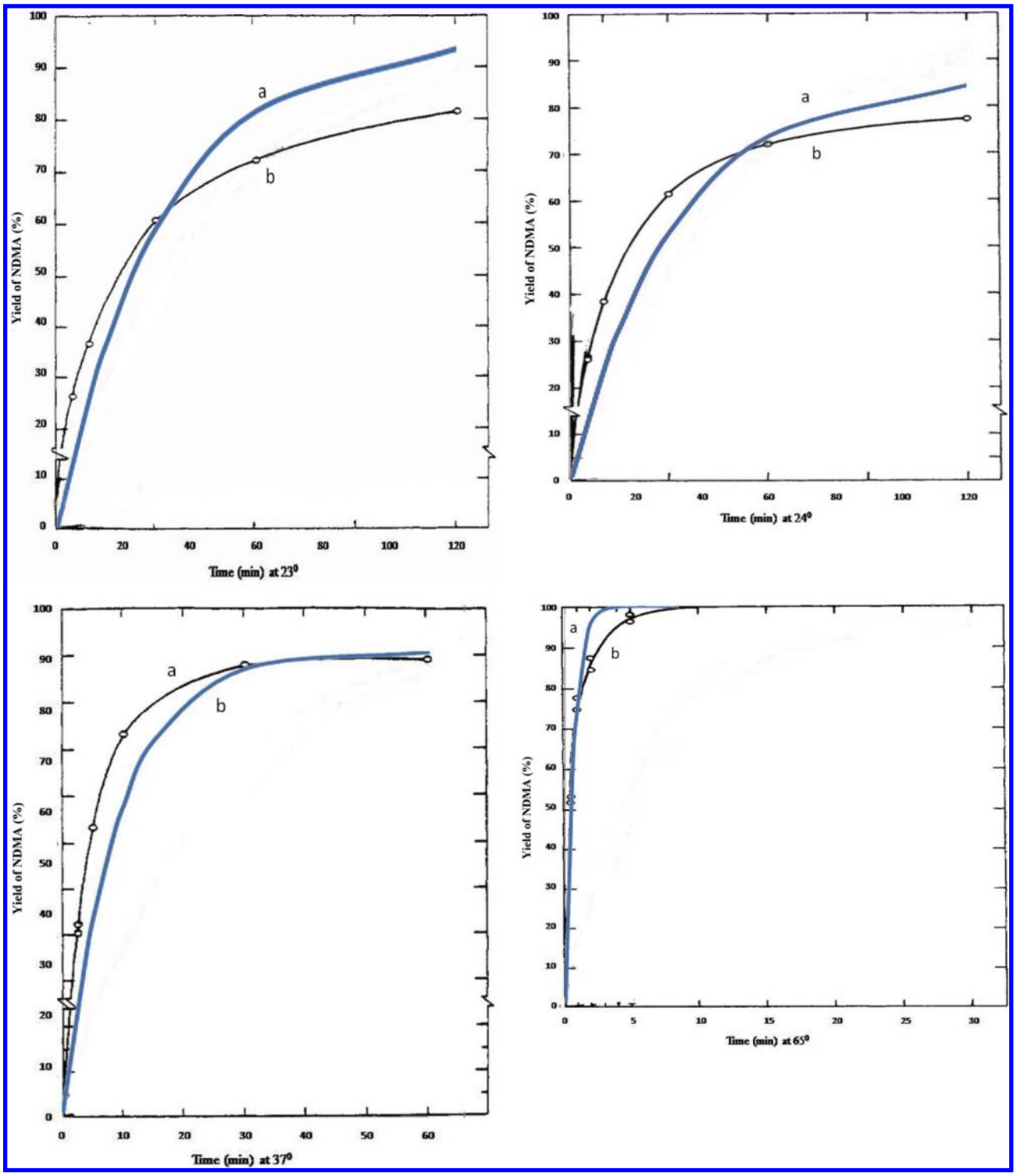

during the reaction of gramine with NO^+ at different levels of *ab initio* theories. Molecular geometries corresponding to the stationary points on the reaction pathway were obtained from the B3LYP/6-311+G(d,p) calculation. Rate constants were reported over the temperature range of 290–360 K using transition state theory. The rate constant of NDMA formation increases with increasing temperature from 23 to 65 °C in the gas phase and in the solution phase.

A similar behavior was found in the experimental work by Mangino and Scanlon.[11] Comparison of data given in Table 2 shows that the rate constant for the first step of NDMA formation (IM1 → IM2) is noticeably faster than that for the second step (IM2 → IM3). The rate constant of the first step is about 3 orders of magnitude larger than the rate of the second step at 290 K at the B3LYP/6-311+G(d,p) level in the gas phase. Therefore, the rate-determining step of NDMA formation is IM2 → IM3.

The rate constants of NDMA formation from gramine calculated at 23, 24, 37, and 65 °C with 1.0 mol L^{-1} nitrite at pH 3.4 show that the results are in good agreement with the experimental results.[11]

References

(1) Magee, P. N.; Barnes, J. M. *Br. J. Cancer* **1956**, *10*, 114. doi:10.1038/bjc.1956.15.
(2) Lijinsky, W.; Epstein, S. S. *Nature* **1970**, *225*, 21. doi:10.1038/225021a0.
(3) Magee, P. N.; Preussmam, R.; Searle, C. E. *Chemical Carcinogens*; American Chemical Society: Washington, DC, 1976; pp 491.
(4) Scanlan, R. A.; Tannenbaum, S. R. *N-Nitroso Compounds*; American Chemical Society: Washington, DC, 1981; pp. 1.
(5) Loeppky, R. N.; Michejda, C. J. *Nitrosamines and Related N-Nitroso Compounds*; Eds., American Chemical Society: Washington, DC, 1994.
(6) Tricker, A. R.; Preussmann, R. *Mutation Res.* **1991**, *259*, 277. doi:10.1016/0165-1218(91)90123-4.
(7) Tricker, A. R.; Preussmann, R. *J. Cancer Res. Clin. Oncol.* **1991**, *117*, 130. doi:10.1007/BF01613136.
(8) Coff, E. U.; Fine, D. H. *Food Cosmet. Toxicol.* **1979**, *17*, 469.
(9) McWeeny, D. J. *Food Chem.* **1983**, *11*, 273.
(10) Billedau, S. M.; Thompson, H. C. *J. Food Sci.* **1988**, *53*, 1696. doi:10.1111/j.1365-2621.1988.tb07818.x.
(11) Mangino, M. M.; Scanlan, R. A. *J. Agric. Food Chem.* **1985**, *33*, 699. doi:10.1021/jf00064a033.
(12) Gower, B. G.; Leete, E. *J. Am. Chem. Soc.* **1963**, *85*, 3683. doi:10.1021/ja00905a034.
(13) Mangino, M. M.; Scanlan, R. A.; Brien, T. J. O. *N-Nitroso Compounds*; American Chemical Society: Washington, DC, 1981; pp. 174.
(14) Rubenchik, B. L. *Carcinogens Formation from Nitrogen Compounds*; Naukova Dumka, Kiev, **1990** (in Russian).
(15) Goodman, L.; Pophristic, V. *Encyclopedia of Computational Chemistry*; Vol. 4, Wiley: New York, 1998.
(16) Gonazales, C.; Schlegel, H. B. *J. Chem. Phys.* **1989**, *90*, 2154. doi:10.1063/1.456010.
(17) Gonazales, C.; Schlegel, H. B. *J. Chem. Phys.* **1990**, *94*, 5523. doi:10.1021/j100377a021.
(18) Fukui, K. *Acc. Chem. Rev.* **1981**, *14*, 363. doi:10.1021/ar00072a001.
(19) Frisch, M. J.; Trucks, G. W.; Schlegel, H. B.; Scuseria, G. E.; Robb, M. A.; Cheeseman, J. R.; Montgomery, J. A., Vreven, T.; Kudin, K. N.; Burant, J. C.; Millam, J. M.; Iyengar, S. S.; Tomasi, J.; Barone, V.; Mennucci, B.; Cossi, M.; Scalmani. G.; Rega, N.; Petersson, G. A.; Nakatsuji, H.; Hada, M.; Ehara, M.; Toyota, K.; Fukuda, R.; Hasegawa, J.; Ishida, M.; Nakajima, T.; Honda, Y.; Kitao, O.; Nakai, H.; Klene, M.; Li, X.; Knox, J. E.; Hratchian, H. P.; Cross, J. B.; Adamo, C.; Jaramillo, J.; Gomperts, R.; Stratmann, R. E.; Yazyev, O.; Austin, A. J.; Cammi, R.; Pomelli, C.; Ochterski, J. W.; Ayala, P. Y.; Morokuma, K.; Voth, G. A.; Salvador, P.; Dannenberg, J. J.; Zakrzewski, V. G.; Dapprich, S.; Daniels, A. D.; Strain, M. C.; Farkas, O; Malick, D. K.; Rabuck, A. D.; Raghavachari, K.; Foresman, J. B.; Ortiz, J. V.; Cui, Q.; Baboul, A. G.; Clifford, S.; Cioslowski, J.; Stefanov, B. B.; Liu, G.; Liashenko, A.; Piskorz, P.; Komaromi, I.; Martin, R. L.; Fox, D. J.; Keith, T.; Al-Laham, M. A.; Peng, C. Y.; Nanayakkara, A.; Challacombe, M.; Gill, P. M. W.; Johnson, B.; Chen, W.; Wong, M. W.; Gonzalez, C; Pople, J.A. *Gaussian 03, Rev. A. l*; Gaussian, Inc.: Pittsburgh, PA, 2003.
(20) Gilbert, R. G.; Smith, S. C. *Theory of Unimolecular and Recombination Reactions*; Blackwell Scientific Publications: Oxford, UK, 1990.
(21) Steinfeld, J. I.; Francisco, J. S.; Hase, W. L. *Chemical Kinetics and Dynamics*; Prentice-Hall: New York, 1998.
(22) Hughes, E. D.; Ingold, C. K.; Ridd, J. H. *J. Chem. Soc.* 1958, 58. doi:10.1039/JR9580000058.
(23) Cossi, M.; Barone, V.; Cammi, R.; Tomasi, J. *Chem. Phys. Lett.* **1996**, *255*, 327. doi:10.1016/0009-2614(96)00349-1.
(24) Miertus, S.; Scrocco, E.; Tomasi, J. *Chem. Phys.* **1981**, *55*, 117.
(25) Miertus, S.; Tomasi, J. J. *Chem. Phys.* **1982**, *65*, 239.
(26) Cossi, M.; Scalmani, G.; Rega, N.; Barone, V. *J. Chem. Phys.* **2002**, *117*, 43. doi:10.1063/1.1480445.
(27) Tissandier, M. D.; Cowen, K. A.; Feng, W. Y.; Gundlach, E.; Cohen, M. H.; Earhart, A. D.; Coe, J. V.; Tuttle, T. R. *J. Phys. Chem. A* **1998**, *102*, 7787. doi:10.1021/jp982638r.